Rigorous Green's Function Formulation for Transmembrane Potential Induced Along a 3-D Infinite Cylindrical Cell

Leonid M. Livshitz, Pinchas D. Einziger, and Joseph Mizrahi*

***Abstract*—The quasi-static electromagnetic field interaction with three-dimensional infinite-cylindrical cell is investigated for both intracellular (IPS) and extracellular (EPS) current point-source excitation. The induced transmembrane potential (TMP), expressed conventionally via Green's function, may alternatively be expanded into a faster-converging representation using a complex contour integration, consisting of an infinite-discrete set of exponentially decaying oscillating modes (corresponding to complex eigenvalues) and a continuous source-mode convolution integral. The dominant contributions for both the IPS and EPS problems are obtained in simple closed-form expressions, including well documented special mathematical functions. In the IPS case, the dominant modal contribution (of order zero)—an exact solution of the well-known cable equation—is explicitly and analytically corrected by the imaginary part of its eigenvalue and the source-mode convolution contribution. However, the TMP along a fiber was shown to decay at infinity algebraically and not exponentially, as predicted by the classic cable equation solution. In the EPS case, the dominant contribution is expressed as a source-mode convolution integral. However, for a long EPS distance (e.g., >10 cable length constant) the order-one-modes involved in the convolution is not a solution of the cable equation. Only for shorter EPS distance should the cable equation solution (i.e., the order zero dominant mode) be included in addition to the modes of order one. For on-membrane EPS location, additional modes should be included as well. In view of our EPS result, we suggest that the cable equation modeling existing in the literature and related to functional electrical stimulation for EPS problems, should be critically reviewed and corrected.**

***Index Terms*—Functional electrical stimulation, Green's function, infinite cylinder, membrane boundary conditions, transmembrane potential (TMP).**

I. Introduction

NERVE cell excitation by an external electric field is an important phenomenon, especially for functional electrical stimulation (FES) applications. A full analysis of the interaction process between electric field and excitable cell presents great difficulties. For this reason, it is recommended [5] to set separate models for the different stages of interaction, i.e.: 1) subthreshold excitation (linear membrane); 2) action potential generation (nonlinear voltage-dependent model); and 3) action potential propagation.

Potential problems arising in nerve and muscle electrophysiology usually are not encountered in the quasi-static electromagnetic theory for the following reasons: 1) internal conductivity of an active fiber is finite and the interior of the fiber is not strictly equipotential and 2) the membrane resistance is generally a function of membrane current flow and the boundary conditions are not linear.

While an applied field is generally modeled as three-dimensional (3-D) and sometimes time-dependent, excitable fiber models are usually one-dimensional (1-D). In addition, compared with a large body of theoretical works on electrodes penetrating a nerve fiber or being in contact with it [1]–[4] there are few available works on remote electrodes. A cell is usually approximated by a finite (spheroidal) or an infinite (cylindrical) geometry. As a subclass of cylindrical models, a 1-D "cable" approximation is widely used [5]–[9]. The classical approach to model an excitable fiber under FES combines 1-D cable theory for pulse propagation, with a membrane model of the Hodgkin–Huxley type [10].

One-dimensional methods have several major flaws. For example, the radial component of the electric field must be taken into account when the current flows into or out of the cell. In cases where circuit models were analyzed it was assumed that the extracellular voltage produced by the stimulating electrode is not distorted by the presence of the cell. It is clear, however, from the quasi-static models [1], that this approximation is weakest immediately outside the cell which is the region of greatest interest to the circuit models. In addition, using finite-size electrodes violates the essential assumption of 1-D cable theory of constant transmembrane potential (TMP) around the cable.

The relation between the cable equation and the zero-order mode of 3-D cylindrical problem with intracellular source location is well-known. In the limit, where the external conductivity approaches infinity, the zero-order mode is an exact solution of the cable equation, as is well documented in the literature (e.g., [11]). Nevertheless, the validity of the cable equation for external problems seems to remain unchallenged.

Three-dimensional theory of biological cell excitation was developed, among others, by Eisenberg and Johnson [2] and Peskoff [3], and summarized by Adrian [11]. Unfortunately, in most of these works the extracellular medium was modeled as a perfect conductor (or insulator), and the electrode was placed

Manuscript received September 7, 2001; revised July 9, 2002. This work was supported by the Isler Foundation. *Asterisk indicates corresponding author.*

L. M. Livshitz is with the Department of Biomedical Engineering, Technion, Israel Institute of Technology, Haifa 32000, Israel (e-mail: jm@biomed.technion.ac.il).

P. D. Einziger is with the Department of Electrical Engineering, Technion, Haifa 32000, Israel.

*J. Mizrahi is with the Department of Biomedical Engineering, Technion, Israel Institute of Technology, Haifa 32000, Israel (e-mail: jm@biomed.technion.ac.il).

Digital Object Identifier 10.1109/TBME.2002.805479

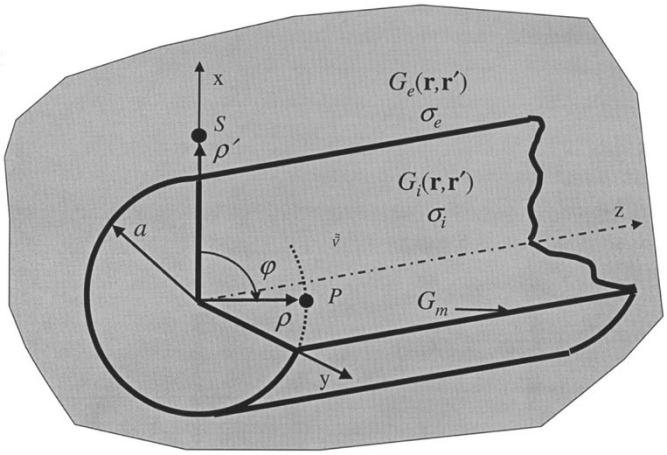

Fig. 1. Physical configuration.

intracellularly. King and Wu [12] analyzed the finite cylindrical fiber model when a constant external electric field was applied.

The present study was initiated to describe the TMP induced by a microelectrode current source placed outside an unmyelinated nerve axon. Mathematically, the steady-state distribution of the potential is given by a Green's function of Laplace equation. The tip of the microelectrode can be represented by a point source, so that Green's function is the potential that one would observe at the membrane. The Green's function satisfies the membrane boundary condition.

The membrane boundary condition is that the normal derivative of the potential at the inside and outside surface of the membrane (proportional to normal component of current) is proportional to some function of the potential difference across the membrane (nonlinear membrane boundary condition). Most authors on the theory of propagated impulse assumed a piecewise linear relation between the membrane current and the membrane potential difference (linear membrane, i.e., impedance boundary condition) [13]. Therefore, we started off with investigating the effects of subthreshold excitation, and assumed that the membrane is purely passive, with no voltage-sensitive conductances and with electrical properties comparable to those of a true fiber near the resting potential.

Thus, this paper deals with finite extracellular conductivity and arbitrary placement of the stimulating electrode. This approach is vital because, during FES, stimulation is extracellular.

II. Integral Representation for TMP

The physical configuration of our problem, depicted in Fig. 1, consists of a source-point S, an observation point P (located on membrane surface), and two cylindrical regions, the axoplasmic core and the surrounding fluid, separated by a thin membrane of radius a. Assuming that the core, the outer fluid and the membrane are homogeneous, isotropic, ohmic conductors, their electrical parameters are denoted by σ_i, σ_e and G_m, respectively. The evaluation of the electrodes' current distributions and potentials is carried out within the quasi-static (low-frequency) regime.

The TMP, i.e., the difference between the internal and external potentials on the membrane surface, is given for a point source excitation as

$$V(\phi, z, \mathbf{r}') = \frac{I}{\sigma(\rho')}\left[G(\mathbf{r}^-, \mathbf{r}') - G(\mathbf{r}^+, \mathbf{r}')\right] \tag{1}$$

where $G(\mathbf{r}, \mathbf{r}')$ denotes the point source response (Green's function). The coordinates $\mathbf{r}' = (\rho', 0, 0)$ and $\mathbf{r} = (a, \phi, z)$ correspond to locations of the source-point S and the observation point P, respectively. The superscripts $+$ and $-$ represent quantities evaluated at the outer and inner surface of the membrane, $\rho = a$, respectively (i.e., $\mathbf{r}^{\pm} = (\rho^{\pm}, \phi, z)$, $\rho^{\pm} = a \pm \varepsilon$, $\varepsilon \to 0$). The point source current is I, and $\sigma(\rho')$ is either σ_i for $\rho' < a$ or σ_e for $\rho' > a$. The Green's function in (1) can be expressed in terms of cylindrical harmonics [14], leading to

$$G(\mathbf{r}, \mathbf{r}') = \frac{1}{2\pi^2}\sum_{n=0}^{\infty}\epsilon_n \cos(n\phi)\int_0^{\infty} g_n(\rho, \rho', k)\cos(kz)\,dk \tag{2}$$

where $\epsilon_0 = 1$ and $\epsilon_n = 2$, $n > 0$. Both $G(\mathbf{r}, \mathbf{r}')$ and $g_n(\rho, \rho', k)$ in (2) satisfy, 3-D and 1-D Laplace equations and appropriate constraints [5], [12], as summarized in Table I.

Substitution of $G(\mathbf{r}, \mathbf{r}')$ in (2) into (1) results in an integral representation for the TMP

$$V(\phi, z, \mathbf{r}') = \frac{I}{2\pi\sigma(\rho')}\sum_{n=0}^{\infty}\epsilon_n V_n(z, \rho')\cos(n\phi) \tag{3}$$

where $V_n(z, \rho')$, the TMP (Fourier's) coefficients, are expressed as

$$V_n(z, \rho') = \frac{1}{\pi}\int_0^{\infty} v_n(\rho', k)\cos(kz)\,dk \tag{4}$$

and $v_n(\rho', k)$, the TMP spectral coefficients, are given via

$$v_n(\rho', k) = g_n(\rho^-, \rho', k) - g_n(\rho^+, \rho', k). \tag{5}$$

The expression for the characteristic Green's function $g_n(\rho, \rho', k)$, obtained after a straightforward but somewhat tedious calculation, is given in Appendix A. The distinguishing subscripts (or superscripts) e and i associated with $\rho' < a$ and $\rho' > a$, respectively (Appendix A) were omitted in (1)–(5) since these equations apply to both extra (EPS) and intracellular current point-source (IPS) excitation locations. This rule is adopted throughout the entire paper for all the equations that apply to both locations. The TMP spectrum for IPS and EPS locations is given via

$$v_n^i(\rho', k) = \left[\frac{I_n(k\rho')}{I_n(ka)}\right]\Big/ q_n(k) \qquad \rho' < a \tag{6}$$

and

$$v_n^e(\rho', k) = \left[\frac{K_n(k\rho')I_n'(ka)}{K_n'(ka)I_n(ka)}\right]\Big/ q_n(k) \qquad \rho' > a \tag{7}$$

respectively. Here, the I_n and K_n are the modified Bessel functions of the order n [15], and prime means differentiation with respect to the argument. The terms in square brackets in both right-hand sides of (6) and (7) represent the point source contribution to the TMP spectrum. Whereas the denominator $q_n(k)$

$$q_n(k) = \frac{G_m a}{\sigma_i} + ka\frac{I_n'(ka)}{I_n(ka)} - \frac{G_m a}{\sigma_e}\frac{K_n(ka)I_n'(ka)}{K_n'(ka)I_n(ka)} \tag{8}$$

TABLE I
POISSON EQUATIONS AND BOUNDARY/MEMBRANE CONDITIONS FOR $G(\mathbf{r},\ \mathbf{r}')$ AND $g_n(\rho,\ \rho',\ k)$

	$G(\mathbf{r}, \mathbf{r}')$	$g_n(\rho, \rho')$
Differential equation	$\nabla^2 G(\mathbf{r}, \mathbf{r}') = -\delta(\mathbf{r} - \mathbf{r}')$	$\left[\frac{1}{\rho}\frac{\mathrm{d}}{\mathrm{d}\rho}\rho\frac{\mathrm{d}}{\mathrm{d}\rho} - k^2 - \frac{n^2}{\rho^2}\right] g_n(\rho, \rho', k) = -\frac{1}{\rho}\delta(\rho - \rho')$
Membrane condition	$G_m[G(\mathbf{r}^-, \mathbf{r}') - G(\mathbf{r}^+, \mathbf{r}')]$ $= -\sigma_e \frac{\partial G(\mathbf{r}^+, \mathbf{r}')}{\partial \rho} = -\sigma_i \frac{\partial G(\mathbf{r}^-, \mathbf{r}')}{\partial \rho}$	$G_m[g_n(\rho^-, \rho', k) - g_n(\rho^+, \rho', k)]$ $= -\sigma_e \frac{\mathrm{d}g_n(\rho^+, \rho', k)}{\mathrm{d}\rho} = -\sigma_i \frac{\mathrm{d}g_n(\rho^-, \rho', k)}{\mathrm{d}\rho}$
Source condition	$\int_{V\to 0} \nabla^2 G(\mathbf{r}, \mathbf{r}') dV = \oint_{A\to 0} \nabla G(\mathbf{r}, \mathbf{r}') \cdot d\mathbf{A} = -1$	$\frac{\mathrm{d}g_n(\rho'^+, \rho', k)}{\mathrm{d}\rho} - \frac{\mathrm{d}g_n(\rho'^-, \rho', k)}{\mathrm{d}\rho} = -\frac{1}{\rho'}$
Decay at infinity	$rG(\mathbf{r}, \mathbf{r}')_{r\to\infty} < \infty$	$\sqrt{\rho}\left[\frac{\mathrm{d}}{\mathrm{d}\rho} + k\right] g_n(\rho, \rho', k)_{\rho\to\infty} = 0$

depends on the intrinsic characteristics of the axon only, namely, its geometry and the associated conductivities (radius a and σ_e, σ_i, G_m, respectively). Therefore, the zeros of the (8), which are essential for the alternative representation of TMP to be carried out next, are independent of the source strength and location.

III. ALTERNATIVE REPRESENTATION

The integral representation (4) in the previous section, representing a continuous summation over each spectral component of the TMP spectrum [the slow convergence is of $O(1/ka)$, since $v_n(\rho',\ k) = O(1/ka)$ as $ka \to \infty$ and $\rho' \to a$], can be expressed alternatively via an equivalent but discrete spectrum, which converges much faster (of exponential order for $z > 0$ and $G_m a/\sigma_e \to 0$, see Appendix C). The alternative representation utilizes ϕ–ρ eigenfunctions expansion guided along the z direction rather than ϕ–z expansion guided along the ρ direction. This is definitely more appropriate for axon propagation problems.

A. IPS: $\rho' < a$

When the alternative representation is performed via contour deformation in complex k space, it is preferable to represent $V_n(z,\ \rho')$ in (4) as

$$V_n^i(z,\ \rho') = \frac{1}{\pi}\,\Re\left[\int_0^\infty v_n^i(\rho',\ k) e^{\jmath k|z|}\, dk\right]. \tag{9}$$

The continuous spectrum representation (in k-space) can be converted into an alternative representation (Appendix B), containing both discrete (dominant) and continuous (minor of $O[(G_m a/\sigma_e)]$) eigenvalues contributions

$$V_n^i(z,\ \rho') = M_n^i(z,\ \rho') + C_n^i(z,\ \rho') \tag{10}$$

where the dominate contribution is

$$M_n^i(z,\ \rho') = \jmath \sum_{m=1}^{\infty} \frac{J_n(\lambda_{n,m}\rho')}{J_n(\lambda_{n,m}a)} \frac{e^{-\lambda_{n,m}|z|}}{q_n'(\jmath\lambda_{n,m})}. \tag{11}$$

The terms in (11) correspond to the pole contribution (residues) at $q_n(k = \jmath\lambda_{n,m}) = 0$ in (8), explicitly

$$q_n(\jmath\lambda_{n,m}) = \frac{G_m a}{\sigma_i} + \lambda_{n,m} a \frac{J_n'(\lambda_{n,m}a)}{J_n(\lambda_{n,m}a)} - \frac{G_m a}{\sigma_e} \frac{H_n^{(2)}(\lambda_{n,m}a) J_n'(\lambda_{n,m}a)}{H_n'^{(2)}(\lambda_{n,m}a) J_n(\lambda_{n,m}a)} = 0 \tag{12}$$

are given via the residue theorem, where $\lambda_{n,m}$ are complex roots of (12) and lie at close vicinity of the real λ-axes (imaginary k-axes, Appendices B and C) [3]. Here, J_n is a Bessel function of the first kind and order n and $H_n^{(2)}$ is a Hankel function of the second kind and order n.

The term $C_n(z,\ \rho')$ can be uniquely represented as a convolution integral, yielding

$$\begin{aligned} C_n^i(z,\ \rho') &= \frac{1}{2\pi}\int_0^\infty v_n^i(\rho',\ k) s_n^i(k) e^{-\jmath k|z|}\, dk \\ &= V_n^i(z,\ \rho') \otimes S_n^i(z) \end{aligned} \tag{13}$$

where the symbol $\otimes$ denotes the convolution operation. The functions $S_n^i(z)$ and $s_n^i(k)$ are given as

$$S_n^i(z) = \frac{1}{2\pi}\int_0^\infty s_n^i(k) e^{-\jmath k|z|}\, dk \tag{14}$$

and

$$\begin{aligned} s_n^i(k) = &-\frac{G_m a}{\sigma_e}\frac{I_n'(ka)}{I_n(ka)} \\ &\times \frac{\jmath\pi(-1)^n}{kaK_n'(ka)[K_n'(ka) - \jmath\pi(-1)^n I_n'(ka)]} \\ &\times \left[\frac{G_m a}{\sigma_i} + ka\frac{I_n'(ka)}{I_n(ka)} - \frac{G_m a}{\sigma_e}\frac{I_n'(ka)}{I_n(ka)} \right. \\ &\left. \times \frac{K_n(ka) - \jmath\pi(-1)^n I_n(ka)}{K_n'(ka) - \jmath\pi(-1)^n I_n'(ka)}\right]^{-1} \end{aligned} \tag{15}$$

respectively (Appendix B). They represent an "activation function" that is related to the external potential. The external potential is a result of the internal potential (and the internal current) leaking out from the fiber due to finite σ_e (Appendix D).

Note that, the continuous spectrum representation in (13) converges faster than integral representation (9), i.e., of $O[(1/ka)^2]$ [rather than $O(1/ka)$ for (9)], as $ka \to \infty$ and $\rho' \to a$. For sufficiently small $G_m a/\sigma_e$, which in practice is always the case, $|s_n^i(k)| < 1$ (Appendix C). Thus, (10) and (13) can be expanded recursively, yielding a converging series representation for $V_n^i(z, \rho')$ in (9)

$$V_n^i(z, \rho') = M_n^i(z, \rho') \otimes \left[\delta(z) + S_n^i(z) + S_n^i(z) \otimes S_n^i(z) + \cdots +\right]. \quad (16)$$

Note that the pth term of the expansion in (16) ($p = 0, 1, \ldots, \infty$) is of $O[(G_m a/\sigma_e)^p]$. The process outlined in (16) can be can be interpreted as follows: the IPS excites internal modes which leak out from the fiber, establishing an external membrane potential. In turn, the resultant "activation function" further excites internal modes (via convolution) and starts the same sequence once more. Each pth iteration (convolution) is of order $(G_m a/\sigma_e)^p$. In the limit $\sigma_e \to \infty$, both the external potential and the resulting "activation function" are zero, which is generally adopted in most of the related textbooks (e.g., [5], [7], [10], and [16]), (16) is reduced into mode expansion only

$$V_n^i(z, \rho') = \overline{M}_n^i(z, \rho') + O(G_m a/\sigma_e) \quad (17)$$

where

$$\overline{M}_n^i(z, \rho') = \sum_{m=1}^{\infty} \frac{J_n(\overline{\lambda}_{n,m}\rho')}{J_n(\overline{\lambda}_{n,m}a)} \frac{\overline{\lambda}_{n,m} e^{-\overline{\lambda}_{n,m}|z|}}{(G_m a/\sigma_i)^2 + (\overline{\lambda}_{n,m}a)^2 - n^2} \quad (18)$$

and $\overline{\lambda}_{n,m}$ is a real-positive mth root of the reduced eigenvalues equation (12)

$$\overline{q}_n(j\lambda_{n,m}) = \frac{G_m a}{\sigma_i} + \overline{\lambda}_{n,m} a \frac{J_n'(\overline{\lambda}_{n,m}a)}{J_n(\overline{\lambda}_{n,m}a)} = 0. \quad (19)$$

Equations (18) and (19) are identical with those obtained, for the limiting case only (i.e., $\sigma_e \to \infty$), in [3], [11], and [17].

B. EPS: $\rho' > a$

The TMP spectrum $v_n^e(\rho', k)$ in (7) can be rewritten in terms of $v_n^i(\rho' = a, k) = q^{-1}(k)$ in (6) as

$$v_n^e(\rho', k) = s_n^e(k) v_n^i(a, k) \quad s_n^e(k) = \frac{K_n(k\rho')I_n'(ka)}{K_n'(ka)I_n(ka)}. \quad (20)$$

Thus, leading to the clear relation between the inner and the outer problems and once more, utilizing $V_n^i(z, a)$ in (16), to a convolution representation for $V_n^e(z, \rho')$ in (6)

$$\begin{aligned} V_n^e(z, \rho') &= \frac{1}{\pi}\int_0^{\infty} s_n^e(k) v_n^i(a, k) \cos(kz)\, dk \\ &= S_n^e(z, \rho') \otimes V_n^i(z, a) \\ &= S_n^e(z, \rho') \otimes M_n^i(z, a) \\ &\quad \otimes [\delta(z) + S_n^i(z) + S_n^i(z) \otimes S_n^i(z) + \cdots +] \\ &= S_n^e(z, \rho') \otimes \overline{M}_n^i(z, a) + O(G_m a/\sigma_e) \end{aligned} \quad (21)$$

where $S_n^e(z, \rho')$ is

$$S_n^e(z, \rho') = \frac{1}{\pi}\int_0^{\infty} s_n^e(k) \cos(kz)\, dk. \quad (22)$$

The discussion following (16) applies here as well, the pth term of the expansion in (21) ($p = 0, 1, \ldots, \infty$) is of $O[(G_m a/\sigma_e)^p]$. Note, however, that the absence of Dirac delta function $\delta(z)$ in (21) prevents a direct excitation of internal modes, but instead provides an "activation function" convolution mechanism only: the EPS establishes an external membrane potential. The resultant "activation function" excites internal modes (via convolution). They leak out from the fiber, establishing an $O[(G_m a/\sigma_e)]$ external membrane potential. In turn, the resultant "activation function" further excites internal modes (via convolution) and starts the same sequence once more. For sufficiently small $G_m a/\sigma_e$, the right-hand side of (21), expressed via (17), is straightforward and represents the dominant $O[1]$ EPS "activation function" convolution contribution to TMP.

IV. TMP Evaluation for the EPS Problem

To complete the alternative representation analysis, discussed in Section III, it is desirable to obtain simple closed-form expressions for the modal expansion as well as for internal and external source-mode convolution integrals in (11), (13) and (21), respectively. The IPS problem is well known and has been investigated rigorously for the case $\sigma_e \to \infty$ (e.g., [5], [7], [10], and [16]) and, thus, extended for finite σ_e in Appendices B–D. Unfortunately, there is no such rigorous documentation for the analysis of the EPS problem. Hence, we focus here on this problem which is crucially important for FES applications. The cases $n = 0$ and $n > 0$ are treated separately.

A. Zero-Order Fourier Coefficient $n = 0$

Generally, closed-form evaluation of either the convolution integral in the right-hand side of (21) or its spectral representation

$$V_0^e(z, \rho') = \frac{1}{\pi}\int_0^{\infty} \frac{s_0^e(k)}{\overline{q}_0(k)} \cos(kz)\, dk + O(G_m a/\sigma_e) \quad (23)$$

for any EPS location (ρ'), is quite cumbersome. Fortunately, for moderately large EPS and observation-point distance (e.g., $\rho' \geq 5a$, as shown in Section V-B) the main contribution to integral (23) comes from the neighborhood of the origin, $k = 0$, since $K_0(k\rho')$ decays exponentially even for small k. The same conclusion also holds for large z in view of the rapid oscillations of the function $\cos(kz)$. In the asymptotic limit $\rho' \gg a$, (23) reduces to

$$\begin{aligned} V_0^e(z, \rho') &\sim \tilde{V}_0^e(z, \rho') \\ &= -\frac{1}{\pi}\int_0^{\infty} \frac{k^2 K_0(k\rho')}{2G_m/(\sigma_i a) + k^2} \cos(kz)\, dk. \end{aligned} \quad (24)$$

Noting that (24) can be rewritten as

$$\tilde{V}_0^e(z, \rho') = \frac{1}{\pi}\frac{\mathrm{d}^2}{\mathrm{d}z^2}\int_0^{\infty} \frac{K_0(k\rho')}{2G_m/(\sigma_i a) + k^2} \cos(kz)\, dk \quad (25)$$

the convolution representation of (24) is

$$\tilde{V}_0^e(z, \rho') = \left[\frac{\mathrm{d}^2}{\mathrm{d}z^2}\tilde{S}_0^e(z, \rho')\right] \otimes \tilde{M}_0^i(z, a) \quad (26)$$

where

$$\tilde{M}_0^i(z,\,a)=\frac{1}{\pi}\int_0^\infty \frac{\cos(kz)}{2G_m/(\sigma_i a)+k^2}\,dk=\frac{\exp(-\overline{\lambda}_{0,\,1}|z|)}{2\overline{\lambda}_{0,\,1}} \tag{27}$$

$\overline{\lambda}_{0,\,1}a=\sqrt{2G_m a/\sigma_i}$ is the lowermost eigenvalue (Appendix C), and

$$\tilde{S}_0^e(z,\,\rho')=\frac{1}{\pi}\int_0^\infty K_0(k\rho')\cos(kz)\,dk=\frac{1}{2(z^2+\rho'^2)^{1/2}}. \tag{28}$$

It should be noted that the cosine transforms of both (28) and (27) are given by closed-form analytic expressions. Here and further on, for evaluation of integral representations, we extensively make use of both the symbolic software *Mathematica 4* (Wolfram Corp., Champaign, IL) and [15]. Both $\tilde{M}_0^i(z,\,a)$ and $\tilde{S}_0^i(z,\,a)$ are closely related to $\overline{M}_0^i(z,\,a)$ and $S_0^e(z,\,a)$, in (18) and (22), respectively

$$\begin{aligned}\frac{a^2}{2}&\left[\overline{M}_0^i(z,\,a)-\sum_{m=2}^{\infty}\frac{\overline{\lambda}_{0,\,m}\exp(-\overline{\lambda}_{0,\,m}|z|)}{(G_m a/\sigma_i)^2+(\overline{\lambda}_{0,\,m}a)^2}\right]\\&=\frac{a^2}{2}\,\frac{\overline{\lambda}_{0,\,1}\exp(-\overline{\lambda}_{0,\,1}|z|)}{(G_m a/\sigma_i)^2+(\overline{\lambda}_{0,\,1}a)^2}\\&=\tilde{M}_0^i(z,\,a)+O(G_m a/\sigma_i)\end{aligned} \tag{29}$$

$$\frac{2}{a^2}\,S_0^e(z,\,\rho')\sim\frac{\mathrm{d}^2}{\mathrm{d}z^2}\,\tilde{S}_0^e(z,\,\rho'). \tag{30}$$

Substituting (27) and (28) into (26) results in

$$\tilde{V}_0^e(z,\,\rho')=\frac{1}{4\overline{\lambda}_{0,\,1}}\,\frac{\mathrm{d}^2}{\mathrm{d}z^2}\int_{-\infty}^{\infty}\frac{\exp(-\overline{\lambda}_{0,\,1}|z-t|)}{(\rho'^2+t^2)^{1/2}}\,\mathrm{d}t. \tag{31}$$

The double differentiation with respect to z can be conveniently performed by subdividing the infinite integration domain $-\infty<t<\infty$ into two semi-infinite domains $-\infty<t\le z$ and $z\le t<\infty$

$$\begin{aligned}\tilde{V}_0^e(z,\,\rho')&=\frac{1}{4\overline{\lambda}_{0,\,1}}\,\frac{\mathrm{d}^2}{\mathrm{d}z^2}\left[\exp(\overline{\lambda}_{0,\,1}z)\int_z^\infty\frac{\exp(-\overline{\lambda}_{0,\,1}t)}{(\rho'^2+t^2)^{1/2}}\,\mathrm{d}t\right.\\&\quad\left.+\exp(-\overline{\lambda}_{0,\,1}z)\int_{-\infty}^{z}\frac{\exp(\overline{\lambda}_{0,\,1}t)}{(\rho'^2+t^2)^{1/2}}\,\mathrm{d}t\right]\\&=\frac{1}{2\overline{\lambda}_{0,\,1}}\,\frac{\mathrm{d}^2}{\mathrm{d}z^2}\left[\cosh(\overline{\lambda}_{0,\,1}z)\int_0^\infty\frac{\exp(-\overline{\lambda}_{0,\,1}t)}{\sqrt{\rho'^2+t^2}}\,\mathrm{d}t\right.\\&\quad\left.-\int_0^z\frac{\sinh[\overline{\lambda}_{0,\,1}(t-z)]}{\sqrt{\rho'^2+t^2}}\,\mathrm{d}t\right]\\&=\frac{1}{2}\left[\overline{\lambda}_{0,\,1}\cosh(\overline{\lambda}_{0,\,1}z)\int_0^\infty\frac{\exp(-\overline{\lambda}_{0,\,1}t)}{\sqrt{\rho'^2+t^2}}\,\mathrm{d}t\right.\\&\quad\left.-\frac{1}{\sqrt{\rho'^2+z^2}}+\overline{\lambda}_{0,\,1}\int_0^z\frac{\sinh[\overline{\lambda}_{0,\,1}(t-z)]}{\sqrt{\rho'^2+t^2}}\,\mathrm{d}t\right].\end{aligned} \tag{32}$$

The first term contained in the right-hand side of (32) can be recognized as

$$\begin{aligned}\int_0^\infty\frac{\exp(-\overline{\lambda}_{0,\,1}t)}{\sqrt{\rho'^2+t^2}}\,\mathrm{d}t&=\int_0^\infty\frac{\exp(-\overline{\lambda}_{0,\,1}\rho' u)}{\sqrt{1+u^2}}\,\mathrm{d}u\\&=\frac{\pi}{2}\left[\mathbb{H}_0(\overline{\lambda}_{0,\,1}\rho')-Y_0(\overline{\lambda}_{0,\,1}\rho')\right]\end{aligned} \tag{33}$$

where $\mathbb{H}_0$ and Y_0 are the zero-order Struve function and Bessel function of the second kind, respectively. The third term, expressed as a definite integral, converges very fast for sufficiently small z/ρ'

$$\begin{aligned}&\overline{\lambda}_{0,\,1}\int_0^z\frac{\sinh[\overline{\lambda}_{0,\,1}(t-z)]}{\sqrt{\rho'^2+t^2}}\,\mathrm{d}t\\&\quad=\overline{\lambda}_{0,\,1}\sum_{p=0}^{\infty}\alpha_p\,\frac{1}{\rho'^{2p+1}}\int_0^z t^{2p}\sinh[\overline{\lambda}_{0,\,1}(t-z)]\,\mathrm{d}t\\&\quad=\overline{\lambda}_{0,\,1}\sum_{p=0}^{\infty}\left(\alpha_p\,\frac{1}{\rho'^{2p+1}}\,\frac{\mathrm{d}^{2p}}{\mathrm{d}\overline{\lambda}_{0,\,1}^{2p}}\int_0^z\sinh[\overline{\lambda}_{0,\,1}(t-z)]\,\mathrm{d}t\right)\\&\quad=\overline{\lambda}_{0,\,1}\sum_{p=0}^{\infty}\alpha_p\,\frac{1}{\rho'^{2p+1}}\,\frac{\mathrm{d}^{2p}}{\mathrm{d}\overline{\lambda}_{0,\,1}^{2p}}\left[\frac{1-\cosh[\overline{\lambda}_{0,\,1}z]}{\overline{\lambda}_{0,\,1}}\right]\\&\quad=[1-\cosh(\overline{\lambda}_{0,\,1}z)]\left\{1+O\left[\left(\frac{z}{\rho'}\right)^2\right]\right\}\\&\quad=-\frac{1}{2\rho'}\left\{(\overline{\lambda}_{0,\,1}z)^2+\frac{(\overline{\lambda}_{0,\,1}z)^4}{12}\left[1-\frac{1}{(\overline{\lambda}_{0,\,1}\rho')^2}\right]\right.\\&\qquad\left.+O[(\overline{\lambda}_{0,\,1}z)^6]\right\}\end{aligned} \tag{34}$$

where

$$\alpha_0=1\quad\text{and}\quad\alpha_p=(-1)^p\,\frac{1\cdot3\cdots(2p-1)}{2\cdot4\cdots2p},\qquad p\ge1.$$

Substituting (33) and (34) back into (32) results in

$$\begin{aligned}\tilde{V}_0^e(z,\,\rho')=\frac{1}{2}\Bigg[&\frac{\overline{\lambda}_{0,\,1}\pi}{2}\cosh(\overline{\lambda}_{0,\,1}z)\left[\mathbb{H}_0(\overline{\lambda}_{0,\,1}\rho')-Y_0(\overline{\lambda}_{0,\,1}\rho')\right]\\&-\frac{1}{\sqrt{\rho'^2+z^2}}+\overline{\lambda}_{0,\,1}\sum_{p=0}^{\infty}\alpha_p\,\frac{1}{\rho'^{2p+1}}\,\frac{\mathrm{d}^{2p}}{\mathrm{d}\overline{\lambda}_{0,\,1}^{2p}}\\&\times\left[\frac{1-\cosh(\overline{\lambda}_{0,\,1}z)}{\overline{\lambda}_{0,\,1}}\right]\Bigg].\end{aligned} \tag{35}$$

The potential $V_0^e(z,\,\rho')$ attains its maximal value at $z=0$. This value can be directly estimated by setting $z=0$ either via (24) or (35), leading to

$$\begin{aligned}\tilde{V}_0^e(0,\,\rho')&=-\frac{1}{\pi}\int_0^\infty\frac{k^2K_0(k\rho')}{2G_m/(\sigma_i a)+k^2}\,dk\\&=\frac{1}{2}\left\{-\frac{1}{\rho'}+\frac{\pi}{2}\,\overline{\lambda}_{0,\,1}\left[\mathbb{H}_0(\overline{\lambda}_{0,\,1}\rho')-Y_0(\overline{\lambda}_{0,\,1}\rho')\right]\right\}.\end{aligned} \tag{36}$$

Replacing $[\mathbb{H}_0(\overline{\lambda}_{0,\,1}\rho')-Y_0(\overline{\lambda}_{0,\,1}\rho')]$ in (36) by its asymptotic expansion for large argument $\overline{\lambda}_{0,\,1}\rho'$ [15]

$$\begin{aligned}&\frac{1}{2}\left\{-\frac{1}{\rho'}+\frac{\pi}{2}\,\overline{\lambda}_{0,\,1}\left[\mathbb{H}_0(\overline{\lambda}_{0,\,1}\rho')-Y_0(\overline{\lambda}_{0,\,1}\rho')\right]\right\}\\&\quad\sim-\frac{1}{2\rho'}\left[\frac{1}{(\overline{\lambda}_{0,\,1}\rho')^2}-\frac{9}{(\overline{\lambda}_{0,\,1}\rho')^4}+\frac{225}{(\overline{\lambda}_{0,\,1}\rho')^6}\right.\\&\qquad\left.+O\left(\frac{1}{(\overline{\lambda}_{0,\,1}\rho')^8}\right)\right]\end{aligned} \tag{37}$$

leads to an explicit dependence of the TMP $V_0^e(0,\,\rho')$ for sufficiently distant EPS location.

B. Higher Order Fourier Coefficients $n > 0$

The evaluation of Fourier coefficients $V_n^e(\rho', z)$ is significantly simplified for $n \geq 1$ and $\rho' \gg a$, since

$$\begin{aligned} V_n^e(z, \rho') &= \frac{1}{\pi}\int_0^\infty \frac{s_n^e(k)}{\overline{q}_n(k)}\cos(kz)\,dk + O(G_m a/\sigma_e) \\ &= \frac{1}{\pi}\int_0^\infty \frac{K_n(k\rho')}{kaK_n'(ka)}\cos(kz)\,dk + O(G_m a/\sigma_e) \\ &\quad + O(G_m a/\sigma_i) \\ &= -\frac{2}{\pi}\int_0^\infty I_n(ka)K_n(k\rho')\left[1-\frac{[K_n(ka)I_n(ka)]'}{2K_n'(ka)I_n(ka)}\right] \\ &\quad \times \cos(kz)\,dk + O(G_m a/\sigma_e) + O(G_m a/\sigma_i). \end{aligned} \tag{38}$$

Asymptotic evaluation of the right-hand side of (38) results in

$$\begin{aligned} V_n^e(z, \rho') &\sim \tilde{V}_n^e(z, \rho') \\ &= -\frac{2}{\pi}\int_0^\infty I_n(ka)K_n(k\rho')\cos(kz)\,dk \\ &= -\frac{1}{\pi\sqrt{a\rho'}}\,Q_{n-1/2}^0\left(\frac{\rho'^2+z^2+a^2}{2a\rho'}\right) \end{aligned} \tag{39}$$

where $Q_n^0(z)$ is the associated Legendre function of the half-integer order of the second kind. Replacing $I_n(ka)$ in (39) by its value for small argument, we obtain

$$\begin{aligned} \tilde{V}_n^e(z, \rho') &= -\frac{1}{\pi\sqrt{a\rho'}}\,Q_{n-1/2}^0\left(\frac{\rho'^2+z^2+a^2}{2a\rho'}\right) \sim \tilde{\tilde{V}}_n^e(z, \rho') \\ &= -\frac{a^n}{\pi 2^{n-1}n!}\int_0^\infty k^n K_n(k\rho')\cos(kz)\,dk \\ &= -\frac{\Gamma(n+1/2)}{\sqrt{\pi}n!}\,\frac{(a\rho')^n}{[z^2+\rho'^2]^{n+1/2}}. \end{aligned} \tag{40}$$

We note that the right-hand side of (40) is an asymptotic evaluation of the associated Legendre function of the half-integer order in (39) for large $\rho'^2 + z^2 \gg a^2$.

The potential $V_n^e(z, \rho')$ attains its maximal value at $z = 0$. This value can be directly estimated via (40) setting $z = 0$

$$\tilde{\tilde{V}}_n^e(0, \rho') = -\frac{\Gamma(n+1/2)}{\sqrt{\pi}n!\rho'}\left(\frac{a}{\rho'}\right)^n. \tag{41}$$

The TMP coefficients $V_n^e(0, \rho')$ for $n = 0$ and $n = 1$ can be obtained directly from (37) and (41), respectively, as

$$\tilde{V}_0^e(z, \rho') = -\frac{1}{2(\overline{\lambda}_{0,1}a)^2\rho'}\left(\frac{a}{\rho'}\right)^2 + O\left[\left(\frac{1}{\lambda_{0,1}\rho'}\right)^4\right] \tag{42}$$

$$\tilde{\tilde{V}}_1^e(z, \rho') = -\frac{1}{2\rho'}\,\frac{a}{\rho'}. \tag{43}$$

Evidently, the zero mode is proportional to the second spatial derivative of the potential while the first-order mode is proportional to its first spatial derivative.

Thus, we can suggest a new rule of thumb to determine whether or not a given fiber will undergo excitation by distant electrode. This rule is based on proportionality to the first or second spatial derivative of the electrode potential (or both) in the *normal* and *tangential* directions with respect to the fiber membrane, respectively, rather than in the *tangential* direction, as suggest in models based on one-dimensional (1-D) cable theory. The exact contributions of different Fourier's coefficients to the TMP will be calculated in Section V.

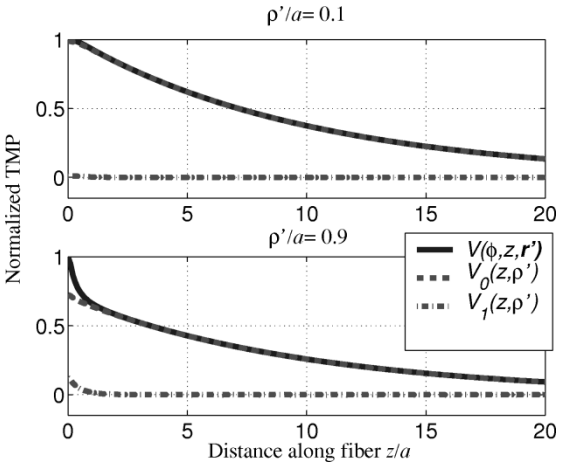

Fig. 2. Normalized TMP for IPS and profiles of its coefficients.

V. Results

For the typical biological case, where the conductivity ratio $G_m a/\sigma_i$ is maintained very low, we have found in the previous section and Appendices A–D that the TMP coefficients (Fourier series coefficients) are insensitive to variations in the σ_e/σ_i. Thus, we used the following passive fiber properties as typical values for running our model $\sigma_i = \sigma_e$, $\sigma_i/G_m a = 200$.

A. TMP and Fourier Harmonics Calculation

Calculation of $V(\phi, z, \mathbf{r}')$ and its Fourier coefficients $V_n(z, \rho')$ for both the EPS and IPS problems are carried out, utilizing (3) and (4).

Fig. 2 shows the normalized TMP distribution along the fiber when the source point is placed intracellularly, either slightly away from the fiber center $\rho'/a = 0.1$ or near the fiber membrane $\rho'/a = 0.9$. As predicted, the plots demonstrate a dominant contribution of the zero-order Fourier harmonics which can be very well approximated via the dominant mode in (18), corresponding to $n = 0$, $m = 1$, and its associated source-mode convolution integral (Appendix B). Only when the electrode is at close vicinity to the membrane, the first order harmonic contributes up to 15% of the total TMP. Note that for large values of z/a, the TMP decays algebraically for finite σ_e values. An exponential decay, associated with the physically unrealistic limit $\sigma_e \to \infty$, leads to concentration of all the leakage current on the outer membrane surface (Appendix B).

Fig. 3 shows the normalized TMP distribution along the fiber when the source point is placed extracellularly at different distances from the fiber, $\rho'/a = 2.5$, 20, 100, and 200. In the close vicinity of the fiber, the harmonics of order zero and one ($n = 0, 1$) contribute dominant portions of the total TMP, but other coefficients (e.g., $n = 2$) are also present. As expected, at distances from the fiber exceeding $100a$ the order-one coefficient ($n = 1$) contributes dominant portions of the total TMP, and the zero order coefficient's contribution becomes small.

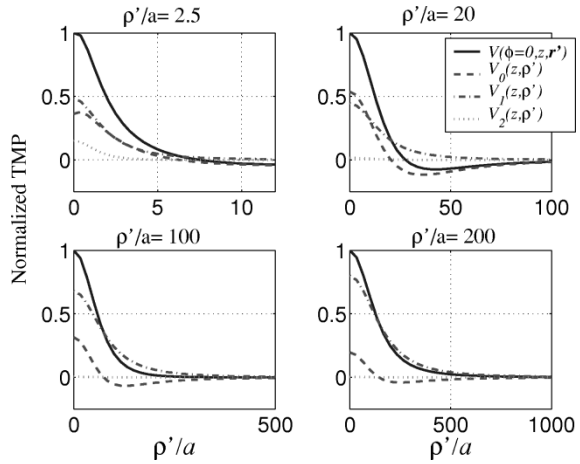

Fig. 3. Normalized TMP for EPS and profiles of its coefficients.

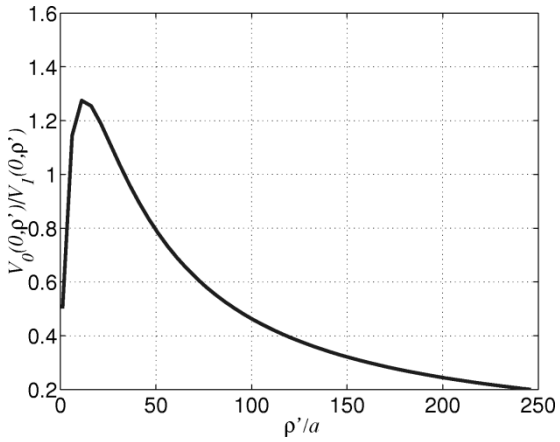

Fig. 4. Ratio of the zero- and first-order harmonics as a function of the fiber/electrode distance at $z = 0$.

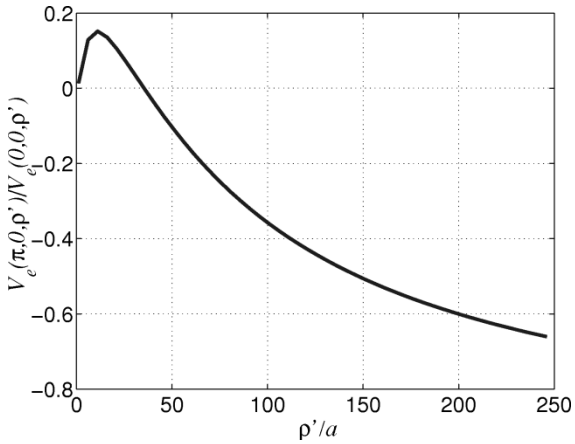

Fig. 5. The ratio of TMP at $z = 0$, on the side of the fiber distant from the electrode ($\phi = \pi$) to TMP on the opposite fiber side (near the electrode, $\phi = 0$) as a function of fiber to source distance.

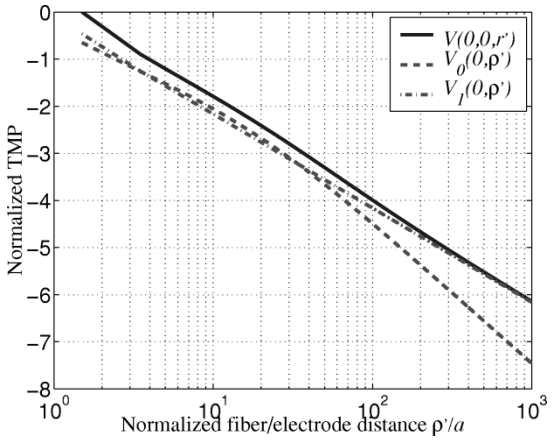

Fig. 6. Normalized TMP and its zero- and first-order coefficients for EPS at $z = 0$ as a function of the fiber electrode distance.

Fig. 4 shows the ratio between the zero-order and first-order harmonics as a function of fiber–source distance at $z = 0$. The plot demonstrates a maximum near $\rho'/a = 10$ and coefficients equality near $\rho'/a = 5$ and $\rho'/a = 35$, but nevertheless up to $\rho'/a = 50$ both coefficients are comparable. The order one coefficient $V_1(z, \rho')$ becomes dominant for distances exceeding 100 fiber diameters. It should be noted that the graph decays as $1/\rho'$ [(42) and (43)].

Fig. 5 shows the ratio of TMP on the side of the fiber distant from the electrode ($\phi = \pi$) to TMP on the opposite fiber side (near the electrode, $\phi = 0$) as a function of fiber to source distance at $z = 0$.

The zero crossing occurs near $\rho'/a = 1$ and $\rho'/a = 35$, due to either division by the source singularity for $\rho'/a = 1$ or $V_e(\pi, 0, 35a) = 0$ since both dominant coefficients $V_0^e(0, 35a)$ and $2V_1^e(0, 35a)$ have the same amplitude and opposite sign at $\phi = \pi$ as can be concluded from Figs. 3 and 4, and the discussion that follows Fig. 4. Thus, the assumption that the variation of the TMP with ϕ along the fiber is not significant, namely the 1-D cable model, is unacceptable.

Fig. 6 shows the variation of the normalized TMP and the zero's and first-order harmonics with fiber–electrode distance at $z = 0$. This is the most important factor for FES application, that directly affects calculation of the activation threshold, and it can serve as a measure of the interaction between electrode and excitable fiber. For distances exceeding $\rho'/a = 35$, the first-order coefficient, which drops as $1/\rho'^2$ [as easily verified from (43) and the semilog presentation of Fig. 6], starts to play a dominant part, and makes the fiber excitation by a distant electrode (fiber–electrode interaction) possible.

B. Verification of Closed-Form Expressions for Fourier Coefficients

In Section V-A, (3) and (4) were rapidly integrated, using an effective discrete cosine transform (DCT) MATLAB routine. Nevertheless, it is useful to have some closed-form expressions for the TMP, that can be further incorporated to nonlinear membrane excitation and action potential propagation models [5], [8], or for macroscopic models such as whole muscle activation [18], [19]. We focus here on the EPS analysis which is most important in practical FES problems, where electrodes are always placed extracellularly. As was shown in Section V-A, the coefficients of order $n = 0$ and $n = 1$ are dominant for most of fiber–electrode distance range. Therefore, without loss of generality, we compare in the following figures plots of the closed-form expressions against numerical calculations of the zero- and first-order Fourier coefficients. Comparisons for

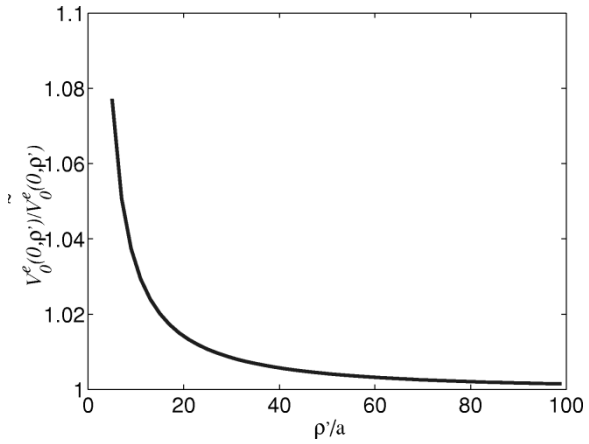

Fig. 7. The ratio at $z = 0$ of the exact cosine transform for the zero-order Fourier coefficient $V_0^e(0, \rho')$ in (36) as function of the fiber–electrode distance.

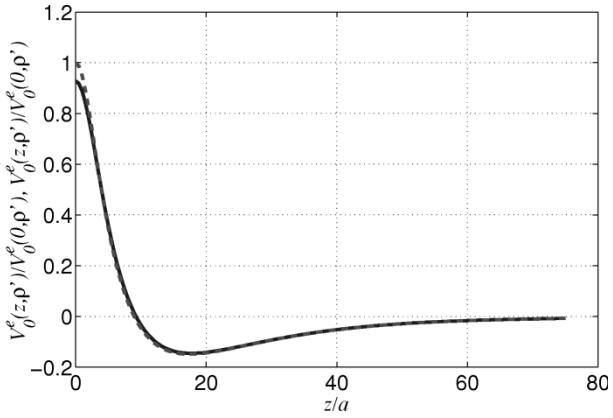

Fig. 8. The exact cosine transform for the zero-order Fourier coefficient and closed-form expression in (35), normalized by $V_0^e(0, \rho')$, along a fiber dashed and solid lines, respectively, as the fiber–electrode distance was held constant at $\rho'/a = 5$.

higher order Fourier coefficients that have been obtained in Section IV can be applied as well.

Fig. 7 shows the ratio between the closed-form expression $\tilde{V}_n^e(0, \rho')$ in (36) and exact cosine transform $V_n^e(0, \rho')$ in (4) as function of fiber–electrode distance at $z = 0$.

Fig. 8 shows the zero-order Fourier coefficients $\tilde{V}_0(z, \rho')$ in (35) and the exact expression $V_0(z, \rho')$ in (4) normalized by $V_0(0, \rho')$, along a fiber. It should be noted that the maximum error appears at $z = 0$. Note that, approximation errors in both Figs. 7 and 8 are smaller than 8%.

Fig. 9 shows the ratio between the exact expression in (4) $V_n^e(z, \rho')$ and the first-order Fourier coefficient $\tilde{V}_n^e(z, \rho')$ and $\tilde{\tilde{V}}_n^e(0, \rho')$ in (39) and (40), respectively, along a fiber at $\rho'/a = 5$. Fig. 10 shows the ratio between the exact expression in (4) $V_n^e(z, \rho')$ and the first-order Fourier coefficient $\tilde{V}_n^e(z, \rho')$ and $\tilde{\tilde{V}}_n^e(0, \rho')$ in (39) and (40), respectively, as a function of fiber–electrode distance at $z = 0$.

Note that the approximation error in both Figs. 9 and 10 is bounded by 8% (as for Figs. 7 and 8). Furthermore, the error data contained in both Figs. 9 and 10 clearly indicate that $\tilde{\tilde{V}}_n^e(0, \rho')$, being a simpler and more accurate closed-form expression, is preferable than $\tilde{V}_n^e(z, \rho')$ (i.e., the associated Legendre function of the half-integer order of the second kind).

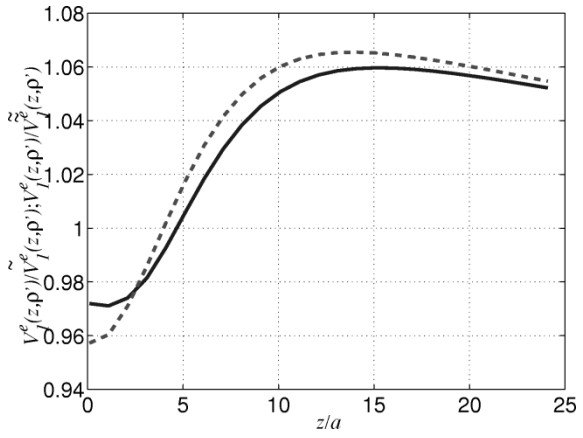

Fig. 9. The ratio of the exact cosine transform for the first-order Fourier coefficients (39) and (40), solid and dashed lines, respectively, along a fiber, as the fiber–electrode distance was held constant at $\rho'/a = 5$.

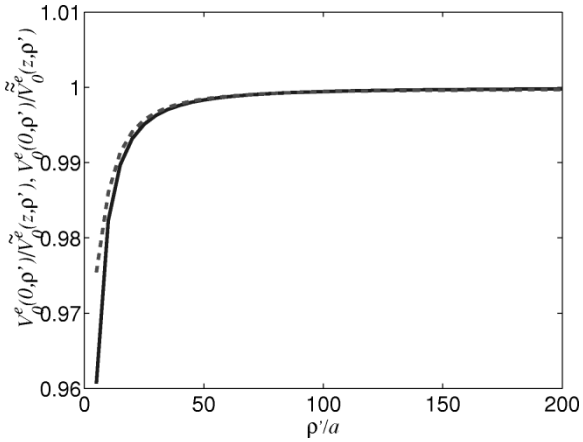

Fig. 10. The ratio at $z = 0$ of the exact cosine transform for the first-order Fourier coefficient $\tilde{V}_1^e(0, \rho')$ in (39) and $\tilde{\tilde{V}}_1^e(0, \rho')$ (40), solid and dashed lines, respectively, as function of fiber–electrode distance.

VI. Summary and Discussion

The quasi-static electromagnetic field interaction with 3-D infinite cylindrical cell was investigated for both IPS and EPS excitations. The induced TMP, expressed conventionally via Green's function, was expanded alternatively into a faster converging representation using a complex contour integration, consisting of an infinite discrete set of exponentially decaying oscillating modes (corresponding to complex eigenvalues) and a continuous source-mode convolution integral.

The TMP was found to be insensitive to large variations of the internal/external conductivity ratio as long as the membrane/internal conductivity ratio is maintained very low. The dominant contribution for both the IPS and EPS problems were obtained in simple closed-form expressions, including well-documented special mathematical functions. In the IPS case, the dominant modal contribution (of order zero)—an exact solution of the well-known cable equation—was explicitly and analytically corrected by the imaginary part of its eigenvalue and the source-mode convolution contribution, both of the order of the membrane/external conductivity ratio. The limit, where the external conductivity approaches infinity is well documented in the literature. In this limit, the convolution integral contribution

vanishes and complex eigenvalues become real. From the model simulation, we concluded that the cable equation is still valid when the axon is stimulated by an internal electrode and the surrounding axoplasm is of finite conductivity. However, the transmembrane potential along a fiber was shown to decay at infinity algebraically and not exponentially, as predicted by the classic cable equation solution.

In the EPS case the dominant contribution was expressed as a source-mode convolution integral. However, for a long EPS distance (e.g., >10 cable length constant) the order-one mode involved in the convolution was not a solution of the cable equation. Only for shorter EPS distance should the cable equation solution (i.e., the order zero dominant mode) be included in addition to the modes of order one. For on-membrane EPS location additional modes should be included as well. In view of our EPS result, we suggest that the cable equation analysis and modeling presented in the existing literature and related to functional electrical stimulation for EPS problems should be critically reviewed and corrected.

There were several attempts in the literature to modify the "activation function" concept [8], [9], [20], [21]. Nevertheless, the validity of the one-dimensional cable equation in the case of *external* electrode excitation via comparison to 3-D model was not completely justified [6].

We maintain that the assumptions on which the application of the cable equation to external stimulation is based, restrict the possibility to apply the "activation function" concept for the case of fiber stimulation by a distant, real-size, electrode. The preliminary analysis of the 3-D cable theory led us to the conclusion that the voltage gradient associated with the current leaving or penetrating the fiber through the membrane can become significant in the close vicinity of the fiber. This result significantly differs from 1-D cable theory.

From the EPS model, it was clear that the zero-order Fourier coefficient is proportional to the second spatial derivative of the potential and the first-order coefficient is proportional to its first spatial derivative. Thus, we can suggest a new rule of thumb to determine whether or not a given fiber will undergo excitation by distant electrode. This rule is based on proportionality to the first or second spatial derivative of the electrode potential (or both) in the *normal* and *tangential* directions with respect to the fiber membrane, respectively, rather than in the *tangential* direction, as suggested in models based on 1-D cable theory.

APPENDIX A
CHARACTERISTIC GREEN'S FUNCTION

A. Internal Point-Source, $\rho' < a$

The characteristic Green's function $g_n^i(\rho, \rho', k)$ for the internal point source, satisfying both the source condition and the decay condition infinity in Table I, is given as [14]

$$g_n^i(\rho, \rho', k) = \begin{cases} I_n(k\rho_<)[A_n(k)I_n(k\rho_>) + K_n(k\rho_>)], & \rho < a \\ B_n(k)I_n(k\rho')K_n(k\rho), & \rho > a \end{cases} \tag{A.1}$$

where $\rho_> \equiv \max(\rho, \rho')$ and $\rho_< \equiv \min(\rho, \rho')$. The coefficients $A_n(k)$ and $B_n(k)$ can be found by applying the membrane condition (Table I)

$$\begin{aligned} &aG_m[A_n(k)I_n(ka) + K_n(ka) - B_n(k)K_n(ka)] \\ &\quad = -\sigma_e kaB(k)K_n'(ka) \\ &aG_m[A_n(k)I_n(ka) + K_n(ka) - B_n(k)K_n(ka)] \\ &\quad = -\sigma_i ka[A_n(k)I_n'(ka) + K_n'(ka)] \end{aligned} \tag{A.2}$$

leading to

$$B_n(k) = \frac{\sigma_i}{\sigma_e}\left[1 + A(k)\,\frac{I_n'(ka)}{K_n'(ka)}\right] \tag{A.3}$$

$$A_n(k) = \left[\frac{aG_mK_n(ka)}{I_n(ka)}\left(\frac{1}{\sigma_e} - \frac{1}{\sigma_i}\right) - \frac{kaK_n'(ka)}{I_n(ka)}\right]\Big/ q_n(k) \tag{A.4}$$

where $q(k)$ is given in (8). Substituting (A.3) and (A.4) into (A.1), results in

$$g_n^i(\rho, \rho', k) = \begin{cases} I_n(k\rho_<)\Big\{I_n(k\rho_>) \times \Big[\dfrac{aG_mK_n(ka)}{I_n(ka)}\left(\dfrac{1}{\sigma_e} - \dfrac{1}{\sigma_i}\right) \\ \quad - \dfrac{kaK_n'(ka)}{I_n(ka)}\Big]\Big/ q_n(k) + K_n(k\rho_>)\Big\}, & \rho < a \\ -\dfrac{aG_mI_n(k\rho')K_n(k\rho)}{ka\sigma_eI_n(ka)K_n'(ka)}\Big/ q_n(k), & \rho > a. \end{cases} \tag{A.5}$$

Thus, evaluating $g_n^i(\rho, \rho', k)$ on the both sides of the membrane

$$g_n^i(\rho, \rho', k) = \begin{cases} \dfrac{I_n(k\rho')}{I_n(ka)}\Big[1 - \dfrac{aG_mK_n(ka)}{ka\sigma_eK_n'(ka)}\Big]\Big/ q_n(k), & \rho = \rho^- \\ -\dfrac{aG_mI_n(k\rho')K_n(ka)}{ka\sigma_eI_n(ka)K_n'(ka)}\Big/ q_n(k), & \rho = \rho^+ \end{cases} \tag{A.6}$$

and taking their difference as outlined in (5), leads to $v_n^i(\rho', k)$ in (6).

B. External Point-Source, $\rho' < a$

Similarly to the IPS case, $g_n^e(\rho, \rho', k)$ for the external point-source, satisfying both the source condition and the decay condition infinity in Table I, is given as

$$g_n^e(\rho, \rho', k) = \begin{cases} A_n(k)I_n(k\rho)K_n(k\rho'), & \rho < a \\ K_n(k\rho_>)[I_n(k\rho_<) + B_n(k)K_n(k\rho_<)], & \rho > a. \end{cases} \tag{A.7}$$

The coefficients $A_n(k)$ and $B_n(k)$ can be found by applying the membrane condition (Table I)

$$\begin{aligned} &aG_m[A_n(k)I_n(k\rho) - I_n(k\rho) - B_n(k)K_n(k\rho)] \\ &\quad = -\sigma_i kaA_n(k)I_n'(k\rho) \\ &\sigma_e[I_n'(k\rho) + B_n(k)K_n'(k\rho)] = \sigma_iA_n(k)I_n'(k\rho) \end{aligned} \tag{A.8}$$

leading to

$$A_n(k) = \frac{\sigma_e}{\sigma_i}\left[1 + B_n(k)\,\frac{K_n'(ka)}{I_n'(ka)}\right] \tag{A.9}$$

and

$$B_n(k) = \left[aG_m\left(\frac{1}{\sigma_e} - \frac{1}{\sigma_i}\right) - ka\,\frac{I_n'(ka)}{I_n(ka)}\right]\frac{I_n'(ka)}{K_n'(ka)}\Big/ q_n(k). \tag{A.10}$$

Substituting (A.10) and (A.9) into (A.7) results in

$$g_n^e(\rho,\,\rho',\,k) = \begin{cases} -\dfrac{aG_m K_n(k\rho')I_n(k\rho)}{ka\sigma_i I_n(ka)K_n'(ka)}\Big/ q_n(k), & \rho < a \\ K_n(k\rho_>)\left\{I_n(k\rho_<) + \left[aG_m\left(\dfrac{1}{\sigma_e} - \dfrac{1}{\sigma_i}\right)\right.\right. & \\ \left.\left. - ka\,\dfrac{I_n'(ka)}{I_n(ka)}\right]\dfrac{I_n'(ka)}{K_n'(ka)}\,K_n'(k\rho_<)\Big/ q_n(k)\right\}, & \rho > a. \end{cases} \tag{A.11}$$

Thus, evaluating $g_n^e(\rho,\,\rho',\,k)$ on the both sides of the membrane

$$g_n^e(\rho,\,\rho',\,k) = \begin{cases} -\dfrac{1}{ka}\,\dfrac{aG_m}{\sigma_i}\,\dfrac{K_n(k\rho')}{K_n'(ka)}\Big/ q(k), & \rho = \rho^- \\ -\dfrac{K_n(k\rho')}{K_n'(ka)}\left[\dfrac{1}{ka}\,\dfrac{aG_m}{\sigma_i} + \dfrac{I_n'(ka)}{I_n(ka)}\right]\Big/ q_n(k), & \rho = \rho^+ \end{cases} \tag{A.12}$$

and taking their difference as outlined in (5), leads to $v_n^e(\rho',\,k)$ in (7).

Appendix B
Eigenfunction and Convolution Expansion of the TMP

Equation (9) can be written in an analytic transformation form as follows:

$$\mathcal{V}_n^i(z,\,\rho') = \frac{1}{\pi}\int_0^\infty v_n^i(\rho',\,k)e^{\jmath k|z|}\,dk. \tag{B.1}$$

Then, utilizing the residue theory in conjunction with Fig. 11, one obtains

$$\mathcal{V}_n^i(z,\,\rho') + \overline{\mathcal{V}}_n^i(z,\,\rho') = 2\pi\jmath\sum_{m=1}^{\infty}\operatorname{Res}\left[\frac{1}{\pi}\,v_n^i(\rho',\,k)e^{\jmath k|z|}\right]_{k=k_{n,\,m}} \tag{B.2}$$

where $\overline{\mathcal{V}}_n^i(z,\,\rho')$ is given as

$$\begin{aligned}\overline{\mathcal{V}}_n^i(z,\,\rho') &= \frac{1}{\pi}\int_{\infty e^{\jmath\pi}}^0 v_n^i(\rho',\,k)e^{\jmath k|z|}\,dk \\ &= \frac{1}{\pi}\int_0^\infty v_n^i(\rho',\,ke^{\jmath\pi})e^{-\jmath k|z|}\,dk\end{aligned} \tag{B.3}$$

and $k_{n,\,m}$ are simple zeros of the eigenvalue equation $q_n(k_{n,\,m}) = 0$. The integration path in (B.3) is just above the branch cut depicted in Fig. 11. Finally, adding and subtracting

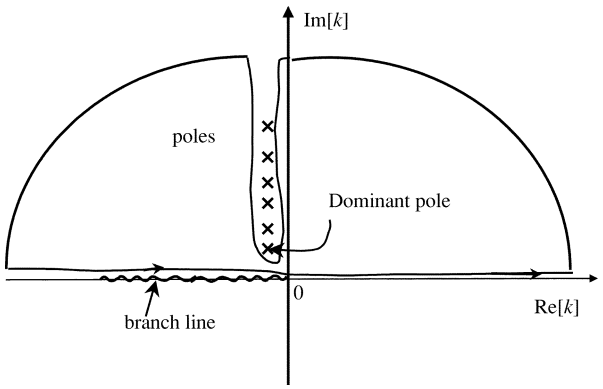

Fig. 11. Contour deformation in the complex k-plane.

the complex conjugate of (B.1) from the left-hand side of (B.2), results in

$$\begin{aligned}V_n^i(z,\,\rho') &= \jmath\sum_{m=1}^{\infty}\operatorname{Res}\left[v_n^i(\rho',\,k)e^{\jmath k|z|}\right]_{k=k_{n,\,m}} \\ &\quad + \frac{1}{2\pi}\int_0^\infty \left[v_n^i(\rho',\,k) - v_n^i(\rho',\,ke^{\jmath\pi})\right]e^{-\jmath k|z|}\,dk \\ &= \jmath\sum_{m=1}^{\infty}\frac{I_n(k_{n,m}\rho')}{I_n(k_{n,m}a)}\,\frac{e^{\jmath k_{n,\,m}|z|}}{q_n'(k_{n,\,m})} \\ &\quad + \frac{1}{2\pi}\int_0^\infty v_n^i(\rho',k)\left[1 - \frac{v_n^i(\rho',ke^{\jmath\pi})}{v_n^i(\rho',k)}\right]e^{-\jmath k|z|}\,dk\end{aligned} \tag{B.4}$$

where prime in $q_n'(k_{n,\,m})$ means differentiation with respect to the argument. Identifying $s_n^i(k)$ as

$$s_n^i(k) = 1 - \frac{v_n^i(\rho',\,ke^{\jmath\pi})}{v_n^i(\rho',\,k)} \tag{B.5}$$

leads to expression (15) and consequently to the convolution relation in (13). The spectral integral either in the right-hand side of (B.4) or in (13) can be evaluated asymptotically, for large z, via end-point integration. The evaluation is carried out by expanding $v_n^i(\rho',\,k)$ and $s_n^i(k)$ in (6) and (15), respectively, in power series at end-point ($k = 0$), leading to

$$C_n^i(z,\,\rho') \sim \begin{cases} \dfrac{\sigma_i}{2\sigma_e}\,\dfrac{\sigma_i}{G_m a}\,\dfrac{1}{a|z/a|^3}, & n = 0 \\ -\dfrac{2}{n}\binom{2n}{n}\left(\dfrac{\rho'}{4a}\right)^n\dfrac{G_m a}{\sigma_e}\,\dfrac{1}{a|z/a|^{2n+1}} & \\ \times\left[1 + O\left(\dfrac{G_m a}{\sigma_e}\right) + O\left(\dfrac{G_m a}{\sigma_i}\right)\right], & n > 0. \end{cases} \tag{B.6}$$

Further simplification of the asymptotic expressions in (B.6) for $n > 0$ have been obtained due to the biological parameter ratio, $G_m a/\sigma_e \ll 1$ (Appendix C). It should be noted that even though the terms corresponding to $n = 0$ and $n = 1$ decay as $1/(z/a)^3$, the zero-order contribution is dominant

$$\left|\frac{C_1^i(z,\,\rho')}{C_0^i(z,\,\rho')}\right| \sim 2\left(\frac{\sigma_e}{\sigma_i}\right)^2\left(\frac{G_m a}{\sigma_e}\right)^2\frac{\rho'}{a} \le 2\left(\frac{\sigma_e}{\sigma_i}\right)^2\left(\frac{G_m a}{\sigma_e}\right)^2 \tag{B.7}$$

since, $G_m a/\sigma_e \ll 1$ whereas $\sigma_e/\sigma_i = O(1)$. Assuming for typical biological data $G_m a/\sigma_e < 10^{-2}$ the right-hand side of (B.7) is less than 10^{-4}.

The asymptotic results for $C_0^i(z, \rho')$ in (B.6) can be extended by including the dominant pole contribution at $\overline{k}_{0,1}a = \jmath\sqrt{2G_m a/\sigma_i} \approx 0$. Indeed, expanding the integrand near $k = 0$ results in

$$\begin{aligned}\Re[C_0^i(z, a)] &\sim -\frac{G_m a}{\sigma_e}\int_0^\infty \frac{(ka)^2\sin(k|z|)\,dk}{[(\overline{\lambda}_{0,1}a)^2 + (ka)^2]^2} \\ &= -\frac{1}{a}\,\frac{G_m a/\sigma_e}{4\overline{\lambda}_{0,1}a}\Big[(1-\overline{\lambda}_{0,1}|z|)e^{-\overline{\lambda}_{0,1}|z|} \\ &\quad\times \overline{\mathrm{Ei}}(\lambda_{0,1}|z|) - (1+\overline{\lambda}_{0,1}|z|)e^{\overline{\lambda}_{0,1}|z|}\mathrm{Ei}(-\overline{\lambda}_{0,1}|z|)\Big]\end{aligned} \tag{B.8}$$

where $\overline{\lambda}_{0,1} = \jmath\overline{k}_{0,1}$, and Ei denotes the exponential integral [15]. As expected

$$\Re[C_0^i(0, a)] \sim 0 \tag{B.9}$$

since $C_0^i(0, a)$ is a Sine transform at $z = 0$, and

$$\Re[C_0^i(z, a)] \sim \frac{\sigma_i}{2\sigma_e}\,\frac{\sigma_i}{G_m a}\,\frac{1}{a|z/a|^3}, \qquad |z| \to \infty \tag{B.10}$$

which is identical to (B.6), setting $n = 0$.

Note that, the TMP decays at infinity $|z| \to \infty$ algebraically and not exponentially, as predicted by the classic cable equation solution. Hence, the leading mode, corresponding to $n = 0$ and $m = 1$, is dominant for $0 < |z| < L = 1/\overline{\lambda}_{0,1}$ (L is the so-called cable length constant), whereas $C_0^i(z, a)$ is dominant for $|z| > L$.

Appendix C
Eigenvalues Determination

A. Numerical Approach

The numerical results of evaluation $\lambda_{n,m}$ of the roots of (12) using routine *fsolve* in Symbolic Toolbox Matlab software are summarized in Fig. 12. The real part of the eigenvalues is negative and very small (typically, $<10^{-5}$). Thus, only the imaginary part is shown. The imaginary part of the eigenvalues is found to be insensitive to large variations of the σ_i/σ_e ratio as long as the conductivity ratio $G_m a/\sigma_i$ is maintained low. The membrane thickness δ and conductivity σ_m are considered to approach zero individually in such a way that the ratio $G_m = \sigma_m/\delta$, the surface conductivity (S/m^2), remains finite. For typical cell used in physiological experiments (nerve axon or muscle fiber), $\delta = 10^{-9}$ m and $a = 5 \div 10 \times 10^{-6}$ m, so that the limit $\delta \to 0$ will lead to no appreciable error on the scale of the cell. Typical values for σ_m and σ_i are 10^{-10} S/m and 10^{-3} S/m, respectively [10]. Hence, the quantity $(\sigma_m/\delta)(a/\sigma_i) = G_m a/\sigma_i$ is less than 10^{-3}.

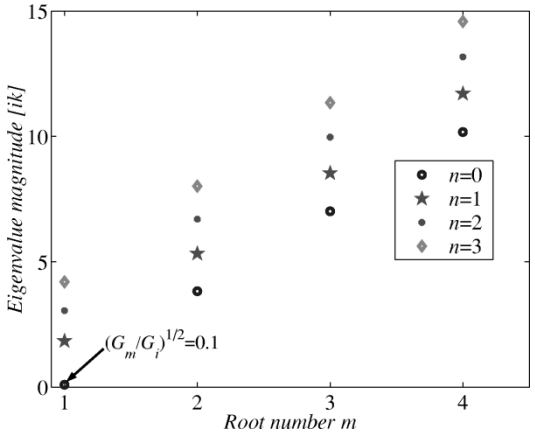

Fig. 12. Eigenvalue locations.

B. Analytic Approach for $n = 0$ and $m = 1$

After expansion of the modified Bessel functions at its small argument value, (8) reads

$$\frac{G_m a}{\sigma_i} + \frac{(ka)^2}{2}\left[1 - \frac{G_m a}{\sigma_e}\ln(ka)\right] = 0. \tag{C.1}$$

Let us define $ka = \rho e^{\jmath\varphi} = \rho\cos(\varphi) + \jmath\sin(\varphi)$ and $\ln(ka) = \ln(\rho) + \jmath\varphi$, where $\jmath$ is the imaginary unit. After separating into the real and image parts, we obtain

$$\begin{cases} 2\,\dfrac{G_m a}{\sigma_i\rho^2}\cos(2\varphi) + 1 - \dfrac{G_m a\ln(\rho)}{\sigma_e} = 0 \\ 2\,\dfrac{G_m a}{\sigma_i\rho^2}\sin(2\varphi) - \dfrac{G_m a\varphi}{\sigma_e} = 0. \end{cases} \tag{C.2}$$

Noting that $0 < \rho \ll 1$, $0 < \varphi < \pi$ and substituting $\varphi = \pi/2 + \delta$ into (C.2), leads to

$$\begin{cases} \varphi = \dfrac{\pi}{2}\left(1 + \dfrac{\sigma_i\rho^2}{\sigma_e}\right) \\ 1 + \rho^2\left(\dfrac{\sigma_i\ln(\rho)}{2\sigma_e} - \dfrac{\sigma_i}{2G_m a}\right) = 0. \end{cases} \tag{C.3}$$

Equation (C.3) represents a system of the two transcendental equations with two unknowns, ρ and φ, gives us solutions for the dominant eigenvalue, that can be found for the specific set of values of σ_e, σ_i, and $G_m a$. For example, for the particular case when σ_e approaches infinity (C.3) reduces to

$$\begin{cases} \varphi = \dfrac{\pi}{2} \\ \rho = \sqrt{2G_m a/\sigma_i}. \end{cases} \tag{C.4}$$

Appendix D
Relation of the Steady-State Cable Equation Solution to Lowest Eigenvalue

A. General Solution of the Cable Equation

The steady-state cable equation [8] reads as follows:

$$\frac{d^2V_m}{dz^2} - R_i\sigma_m V_m = -\frac{d^2V_e}{dz^2}\bigg|_{a+}. \tag{D.1}$$

Note that $R_i = 1/(\pi a^2 \sigma_i)$ and $\sigma_m = G_m 2\pi a$ both per unit length. The homogeneous solution is

$$V_{mh} = Ae^{-\overline{\lambda}_{0,1} z} + Be^{\overline{\lambda}_{0,1} z}$$
$$\overline{\lambda}_{0,1} a = \sqrt{R_i \sigma_m} a = \sqrt{2G_m a/\sigma_i}. \tag{D.2}$$

Green's function for the cable equation is define via

$$\frac{d^2 g_m}{dz^2} - R_i \sigma_m g_m = -\delta(z) \tag{D.3}$$

i.e.,

$$g_m = \frac{e^{-\overline{\lambda}_{0,1}|z|}}{2\overline{\lambda}_{0,1}}. \tag{D.4}$$

Thus, the particular solution is given as

$$V_{mp} = \frac{d^2 V_e}{dz^2} \otimes g_m. \tag{D.5}$$

The general solution is

$$V_m = V_{mp} + V_{mh}. \tag{D.6}$$

B. Relation of the Lowest Eigenfuction ($n = 0$, $m = 1$) to the Cable Equation and "Activation Function" IPS Case [7]

Substitution of (B.8) into (D.1)

$$\left(\frac{d^2}{dz^2} - \overline{\lambda}_{0,1}^2\right) \Re[C_0^i(z, \rho')] = -\frac{d^2 V_e}{dz^2} \tag{D.7}$$

results in

$$-\frac{d^2 V_e}{dz^2} = \frac{G_m a}{a^2 \sigma_e} \int_0^\infty \frac{(ka)^2 \sin(k|z|)}{(\overline{\lambda}_{0,1} a)^2 + (ka)^2}\, dk$$
$$= -\frac{G_m a}{\sigma_e} \frac{d^2}{dz^2} \int_0^\infty \frac{\sin(k|z|)}{(\overline{\lambda}_{0,1} a)^2 + (ka)^2}\, dk \tag{D.8}$$

where [see (B.8)]

$$V_e = \frac{G_m a}{\sigma_e} \int_0^\infty \frac{\sin(k|z|)}{(\overline{\lambda}_{0,1} a)^2 + (ka)^2}\, dk$$
$$= \frac{G_m a}{2\sigma_e \overline{\lambda}_{0,1} a} \left[e^{-\overline{\lambda}_{0,1}|z|} \overline{\mathrm{Ei}}(\overline{\lambda}_{0,1}|z|) - e^{\overline{\lambda}_{0,1}|z|} \mathrm{Ei}(-\overline{\lambda}_{0,1}|z|)\right]. \tag{D.9}$$

Combining both (D.9) and (18) [or (29)], one obtains the complete cable equation for the IPS problem

$$\left(\frac{d^2}{dz^2} - \overline{\lambda}_{0,1}^2\right) V_m = -\frac{2}{a^2}\, \delta(z) - \frac{d^2 V_e}{dz^2}. \tag{D.10}$$

It should be noted that the $O(G_m a/\sigma_e)$ correction to the impulse response in (18) [or (29)] has been ignored, since either it is insignificant for $0 < |z| < L = 1/\overline{\lambda}$ or $C_0^i(\rho', a)$ is dominant for $|z| > L$.

Finally, the internal current $I_i(z)$ can be efficiently approximated, via the dominant mode ($n = 0$, $m = 1$) contribution

$$I(z) = \frac{1}{R_i} \frac{I}{2\pi\sigma_i} \frac{dV_m(z)}{dz}$$
$$= \frac{I}{2} e^{-\overline{\lambda}_{0,1}|z|} + O\left(\frac{G_m a}{\sigma_e}\right). \tag{D.11}$$

REFERENCES

[1] J. Bernhardt and H. Pauly, "On the generation of potential differences across the membranes of ellipsoidal cells in an alternating current," *Biophysik*, vol. 10, pp. 89–98, 1973.

[2] R. S. Eisenberg and E. A. Johnson, "Three-dimensional electrical field problem in physiology," *Prog. Biophys. Mol. Biol.*, vol. 20, pp. 1–65, 1970.

[3] A. Peskoff, "Green's function for Laplace equation in an infinite cylindrical cell," *J. Math. Phys.*, vol. 15, no. 12, pp. 2112–2120, 1974.

[4] O. Sten-Knudsen, "Is muscle contraction initiated by internal current flow," *J. Physiol.*, vol. 151, pp. 363–384, 1960.

[5] J. J. B. Jack, D. Noble, and R. W. Tsien, *Electric Current Flow in Excitable Cells*. Oxford, U.K.: Claredon, 1988, pp. 99–129.

[6] D. R. McNeal, "Analysis of a model for excitation of myelinated nerve," *IEEE Trans. Biomed. Eng.*, vol. BME-23, pp. 329–337, Apr. 1976.

[7] F. Rattay, *Electrical Nerve Stimulation*. New York: Springer-Verlag, 1990.

[8] E. N. Warman, W. M. Grill, and D. M. Durand, "Modeling the effects of electric fields on nerve fibers: Determination of excitation thresholds," *IEEE Trans. Biomed. Eng.*, vol. 39, pp. 1244–1254, Dec. 1992.

[9] C. M. Zierhofer, "Analysis of a linear model for electrical stimulation of axons—Critical remarks on the 'activating function concept'," *IEEE Trans. Biomed. Eng.*, vol. 48, pp. 173–184, Feb. 2001.

[10] J. P. Reilly, *Applied Bioelectricity*. New York: Springer-Verlag, 1998.

[11] R. H. Adrian, "Electrical properties of striated muscle," in *Handbook of Physiology*, L. Peachy, Ed. Bethesda, MD: Amer. Phys. Soc., 1983, ch. 10, Skeletal Muscle, sec. X, pp. 275–300.

[12] R. W. P. King and T. T. Wu, "Electric field induced in cells in the human body when this is exposed to low-frequency electric field," *Phys. Rev. E*, vol. 58, no. 2, pp. 2363–2369, 1998.

[13] A. M. Weinberg, "Green's function in biological potential problem," *Bull. Math. Biophys.*, vol. 4, pp. 107–115, 1942.

[14] J. D. Jackson, *Classical Electodynamics*, 3rd ed. New York: Wiley, 1999.

[15] I. S. Gradstein and I. M. Ryzhik, *Table of Integrals, Series, and Products*. New York: Academic, 1965.

[16] R. Plonsey and R. E. Barr, "Electric field stimulation of excitable tissue," *IEEE Trans. Biomed. Eng.*, vol. 42, pp. 329–336, Apr. 1995.

[17] H. S. Carslaw, *Mathematical Theory of the Conduction of Heat in Solids*. New York: Dover, 1945.

[18] L. M. Livshitz, P. D. Einziger, and J. Mizrahi, "Current distribution in skeletal muscle activated by FES: Image-series formulation and isometric recruitment curve," *Ann. Biomed. Eng.*, vol. 28, pp. 1218–28, 2000.

[19] L. M. Livshitz, J. Mizrahi, and P. D. Einziger, "Interaction of array of finite electrodes with layered biological tissue: Effect of electrode size and configuration," *IEEE Trans. Neural Syst. Rehab. Eng.*, vol. 9, pp. 355–361, Aug. 2001.

[20] J. Ruohonen, M. Panizza, J. Nilsson, P. Ravazzani, F. Grandori, and G. Tognola, "Transverse-field activation mechanism in magnetic stimulation of peripheral nerves," *Electroenceph. Clin. Neurophys.*, vol. 101, pp. 167–174, 1996.

[21] V. Schnabel and J. J. Struijk, "Calculation of electric fields in a multiple cylindrical volume conductor induced by magnetic coils," *IEEE Trans. Biomed. Eng.*, vol. 48, pp. 78–86, Jan. 2001.

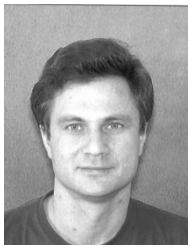

Leonid M. Livshitz received the B.S. degree in electrical engineering from the Moscow State University of Railway Transport (MIIT), Moscow, Russia, and the M.S. and Ph.D. degrees in biomedical engineering from the Technion—Israel Institute of Technology, Haifa, Israel, in 1986, 1997, and 2002, respectively.

From 1986 to 1991, he worked as a Computer and Electrical Engineer at the Moscow Transport University, Moscow, Russia. His research interests include computational aspects of the interaction between applied electrical and magnetic fields with nerves and muscles, functional electrical stimulation of muscles, and muscle excitation–contraction coupling.

Pinchas D. Einziger received the B.Sc. and M.Sc. degrees in electrical engineering from the Technion—Israel Institute of Technology, Haifa, Israel, and the Ph.D. degree in electrophysics from the Polytechnic University, Brooklyn, NY, in 1976, 1978, and 1981, respectively.

Since 1981, he has been on the Faculty of the Department of Electrical Engineering at the Technion. His main interests are electromagnetic wave theory, nonlinear wave phenomena, and bioelectromagnetics.

Joseph Mizrahi received the B.Sc. degree in aeronautical engineering, the M.Sc. degree in mechanics, and the D.Sc. degree in biomechanics, all from the Technion—Israel Institute of Technology, Haifa, Israel, in 1967, 1970, and 1975, respectively.

He is currently Professor and Incumbent of the Pearl Milch Chair of Biomedical Engineering Sciences in the Department of Biomedical Engineering, Technion. For 18 years, he was head of the Biomechanics Laboratory at the Loewenstein Rehabilitation Center, Raanana, Israel. He also held several visiting professorships, including with the Harvard Medical School, Cambridge, MA, (1989–1990), the University of Cape Town, South Africa, (1991) and the Hong Kong Polytechnic University (1998–1999), Hong Kong. He is principal author of some 200 publications, and he presently holds several editorial responsibilities. His major research interests are in orthopaedic biomechanics and electrical stimulation of muscles.